EMBO
reports

TRANSPARENT
PROCESS

Xanthomonas campestris attenuates virulence by sensing light through a bacterio-phytochrome photoreceptor

Hernán R Bonomi[1,*], Laila Toum[2], Gabriela Sycz[1], Rodrigo Sieira[1], Andrés M Toscani[3], Gustavo E Gudesblat[2], Federico C Leskow[3], Fernando A Goldbaum[1], Adrián A Vojnov[2,**] & Florencia Malamud[2,4,***]

Abstract

Phytochromes constitute a major photoreceptor family found in plants, algae, fungi, and prokaryotes, including pathogens. Here, we report that *Xanthomonas campestris* pv. *campestris* (*Xcc*), the causal agent of black rot disease which affects cruciferous crops worldwide, codes for a functional bacteriophytochrome (*Xcc*BphP). *Xcc*BphP possesses an N-terminal PAS2-GAF-PHY photosensory domain triad and a C-terminal PAS9 domain as its output module. Our results show that illumination of *Xcc*, prior to plant infection, attenuates its virulence in an *Xcc*BphP-dependent manner. Moreover, in response to light, *Xcc*BphP downregulates xanthan exopolysaccharide production and biofilm formation, two known *Xcc* virulence factors. Furthermore, the *XccbphP* null mutant shows enhanced virulence, similar to that of dark-adapted *Xcc* cultures. Stomatal aperture regulation and callose deposition, both well-established plant defense mechanisms against bacterial pathogens, are overridden by the *XccbphP* strain. Additionally, an RNA-Seq analysis reveals that far-red light or *Xcc*BphP overexpression produces genomewide transcriptional changes, including the inhibition of several *Xcc* virulence systems. Our findings indicate that *Xcc* senses light through *Xcc*BphP, eliciting bacterial virulence attenuation via downregulation of bacterial virulence factors. The capacity of *Xcc*BphP to respond to light both *in vitro* and *in vivo* was abolished by a mutation on the conserved Cys13 residue. These results provide evidence for a novel bacteriophytochrome function affecting an infectious process.

Introduction

Biological photoreceptors are found in all kingdoms of life. They can detect the wavelength, duration, direction, and intensity of light and consequently transduce this information within cells to exert the corresponding biological outputs. Photoreceptors from photosynthetic autotrophs were the first to be identified and described, and were subsequently discovered in non-photosynthetic organisms [1,2]. However, it was not until recently that they were reported to be functional *in vivo* in auxotrophic bacteria. In fact, several studies show that these proteins are key elements in bacterial physiology. Interestingly, it is the case of the blue-light photoreceptors containing LOV (light, oxygen, voltage) domains that are known to regulate the infectious processes in some bacteria [3–5], among other activities.

Phytochrome photoreceptors can be found in plants, eukaryotic algae, fungi, and photosynthetic and non-photosynthetic prokaryotes [6,7]. They are reversibly photoconverted, typically, between a red-absorbing (Pr) and a far-red-absorbing (Pfr) state [8]. These photoreceptors were originally discovered in plants where they are recognized to regulate many key processes [9,10]; subsequently, their bacterial homologues, bacteriophytochromes (BphPs), were identified [11,12]. Interestingly, BphPs have been linked to some bacterial physiological responses [13,14], yet most of the biological processes they regulate are still elusive.

Xanthomonas campestris pv. *campestris* (*Xcc*), a non-photosynthetic phytopathogenic bacterium distributed worldwide, is responsible for the so-called black rot disease in cruciferous plants,

1 Fundación Instituto Leloir − IIBBA CONICET, Buenos Aires, Argentina
2 Instituto de Ciencia y Tecnología Dr. Cesar Milstein, Fundación Pablo Cassará, CONICET, Buenos Aires, Argentina
3 Departamento de Química Biológica, Facultad de Ciencias Exactas y Naturales, Universidad de Buenos Aires, Buenos Aires, Argentina
4 UNSAM Campus Miguelete IIB - Instituto de Investigaciones Biotecnológicas, Buenos Aires, Argentina
  *Corresponding author. Tel: +54 11 5238 7500; E-mail: hbonomi@leloir.org.ar
  **Corresponding author. Tel: +54 11 4105 4100; E-mail: avojnov@fundacioncassara.org.ar
  ***Corresponding author. Tel: +54 11 4006 1500; E-mail: fmalamud@iibintech.com.ar

causing huge economic loses [15,16]. This pathogen has the ability to live epiphytically and also colonize the plant xylem by entering through the stomata or wounds [17]. During the epiphytic stage, bacteria are exposed to nutrient limitation, fluctuating water availability, exposure to sunlight containing ultraviolet radiation, and subjected to the diurnal light cycle [18]. The effect of light has been extensively studied in phototrophic bacteria and only recently examined in non-phototrophic bacteria.

The *Xcc* genome codes for two identified photoreceptors, a LOV domain histidine kinase protein and a BphP. The purpose of this study was to determine the functionality of the *Xanthomonas* bacteriophytochrome photoreceptor, here designated *Xcc*BphP, and whether it plays a significant role in bacterial virulence.

Results

Xcc codes for a functional bacteriophytochrome

The *XccbphP* gene is located downstream from a heme oxygenase-coding gene (*XccbphO*) forming a bicistronic operon (Fig 1A), as similarly found in other bacteria [19]. The heme oxygenase enzyme is known to catalyze the conversion of heme into biliverdin-IXα (BV), the open-chain tetrapyrrole bilin chromophore bound in BphPs [8]. In order to determine whether the *XccbphO–XccbphP* operon is functional *in vivo*, we performed RT–PCR from *Xcc* RNA purifications, confirming that it is actively transcribed and that there is a physical linkage between *XccbphO* and *XccbphP* mRNAs (Fig 1B). Moreover, *Xcc*BphP was detected in wild-type extracts by SDS–PAGE and Western blotting displaying the expected molecular weight (Fig EV1B).

The *Xcc*BphP sequence displays four conserved domains (Fig 1C): Per/Arndt/Sim (PAS2 family), cGMP phosphodiesterase/adenyl cyclase/FhlA (GAF), phytochrome-associated (PHY), and output/effector module (PAS9 family), according to a Pfam database classification [20]. The PAS2–GAF–PHY triad represents the photosensory module involved in BV binding, where the PAS2 domain bears a conserved cysteine at position 13 involved in the covalent chromophore linkage [21,22]. It is the BV chromophore buried in the protein structure that allows phytochromes to reversibly photoconvert between red-absorbing (Pr) and far-red-absorbing (Pfr) states by photoisomerization. The PAS9 domain from *Xcc*BphP bears no predicted enzymatic activity; moreover, PAS domains are recognized to mediate interactions between proteins in signaling systems [23]. The three-domain photosensory module, typically coupled with an output module, is a conserved feature of *bona fide* phytochromes, and it can be found among phytochromes across different kingdoms of life comprising plant, fungi, algae, and bacteria, even while sharing low sequence identity. The composition of the output module varies among phytochromes and would govern the nature of the downstream signaling after light-sensing events by the photosensor (Table EV1). To investigate the extent of BphP occurrence in the *Xanthomonas* genus, we identified all *Xcc*BphP homologous sequences bearing a PAS2–GAF–PHY photosensory module within the genus in UniProtKB database. A total of 75 different sequences were found from a wide variety of plant pathogenic *Xanthomonas* spp. exhibiting only five categories of output module domain sequences: (i) PAS4,
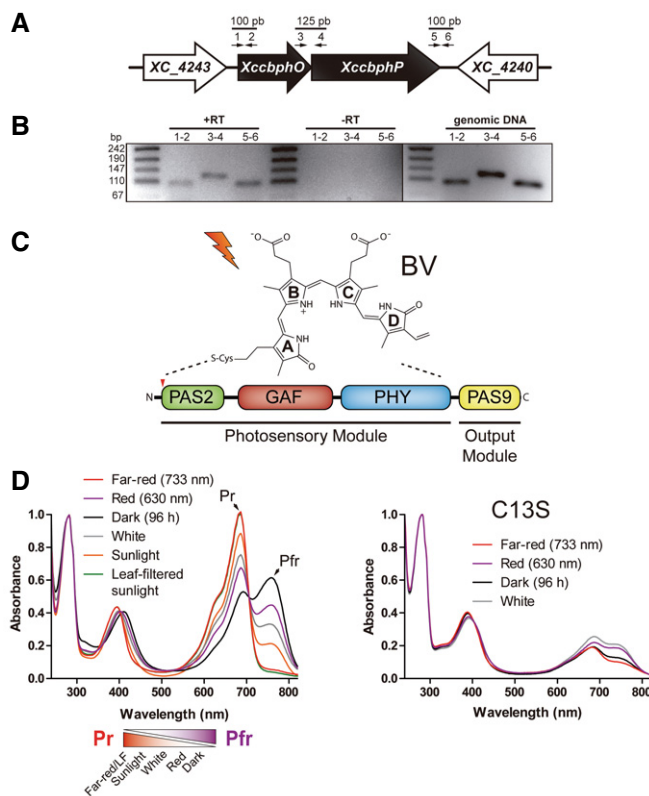

Figure 1. *Xcc*BphP genomic organization, domain topology, and UV–vis spectral properties.

A The *XccbphP* gene (XC_4241) is located downstream the heme oxygenase gene (*XccbphO*) as a bicistronic operon. Specific primers (small numbered arrows) were designed to evaluate the physical linkage between *XccbphO* and *XccbphP* mRNAs.

B The confirmative RT–PCRs were resolved in a 2% agarose gel. Untreated reverse transcriptase RNAs (-RT) and genomic DNA served as negative and positive controls, respectively.

C The *Xcc*BphP domain architecture. The photosensory module, composed by the PAS2-GAF-PHY domain triad, binds to the chromophore biliverdin-IXα (BV) from a conserved cysteine residue indicated by a red arrow (Cys13). The output module comprises a single PAS9 domain.

D Left panel: Absorption spectra of dark-adapted *Xcc*BphP after illumination with red, far-red, fluorescent white lamp light, sunlight, or sunlight filtered through green leaves (LF). Pr/Pfr equilibrium scheme derived from absorption spectra is depicted in the bottom panel. Right panel: The *Xcc*BphP-C13S mutant was purified in the presence of BV and its absorption spectra recorded upon illumination with red, far-red, and white light or dark adaptation.

(ii) PAS8, (iii) PAS9, (vi) histidine kinase (HisKA subfamily), and (v) absence of any conserved domain (Fig EV2). Single PAS domains correspond to almost 95% of the *Xanthomonas* BphP output modules, PAS4 being the most abundant (64%), followed by PAS9 (~21%) and PAS8 (~9%). Only two BphPs were found to bear a histidine kinase module, and two sequences did not show any recognizable output module.

Recently, the *Xcc*BphP structure and basic photochemistry have been reported, demonstrating its capacity to function as a red/far-red light photoreceptor *in vitro* [22]. We sought to further characterize *Xcc*BphP spectroscopically. For that aim, recombinant full-length *Xcc*BphP holoprotein was purified. BV bound to the

photosensory module was evidenced by the presence of the Soret and Q bands (Abs_{400}/Abs_{750}) in the UV–vis absorption spectrum (Fig 1D). As expected, far-red (733 nm) irradiation leads to a photoconversion of the holoprotein into a pure Pr species, indicated by a maximum absorption peak at 688 nm and the lack of the Pfr absorption band at 752 nm (Fig 1D). Irradiation with red (630 nm) and fluorescent white light lamp promotes the appearance of the Pfr form, corresponding to a Pfr:Pr ratio calculated of ~2 and ~1, respectively. In the dark, thermal conversion leads to the accumulation of the Pfr state exhibiting a final Pfr:Pr ratio calculated of ~6 at 21 h (Fig 1D). A Pr ground state and a dark conversion from Pfr to Pr are characteristic of prototypical phytochromes. Conversely, the bathytype phytochromes exhibit a Pfr ground state and a Pr to Pfr dark conversion [24,25]. Therefore, *Xcc*BphP fits into the bathy-type phytochrome category, although an incomplete Pr-to-Pfr dark conversion and a Pr/Pfr equilibrium are observed. Interestingly, when *Xcc*BphP apoprotein is incubated with BV in the dark, the holoprotein is first constituted as pure Pr but then reaches the same Pfr:Pr ratio of ~6 [22]. To simulate natural conditions, *Xcc*BphP was exposed to direct sunlight or sunlight filtered through green leaves mimicking a canopy. Sunlight alone promotes a photoreceptor Pr enrichment with a Pr:Pfr ratio of ~3, contrary to the Pfr enrichment observed in dark equilibrium. Moreover, when *Xcc*BphP was subjected to leaf-filtered sunlight a pure Pr spectrum could be observed (Fig 1D), similar to the one obtained after artificial far-red LED irradiation. The functionality of the conserved cysteine residue at the PAS2 domain was addressed by constructing an *Xcc*BphP point mutant replacing Cys13 by a serine residue (*Xcc*BphP-C13S) and evaluating its spectroscopic properties. Although *Xcc*BphP-C13S still retains binding to BV, as evidenced by its absorption spectrum, it exhibits no photo-inducible Pr-Pfr changes (Fig 1E). Hence, the presence of Cys13 is necessary for the correct *Xcc*BphP photoactivity.

*Xcc*BphP negatively regulates *Xcc* virulence in a light-dependent manner

To test the role of *Xcc*BphP in *Xcc* virulence, we first generated a null mutant (*XccbphP*) by an allelic replacement of the XC_4241 ORF with an antibiotic resistance (Sm^r/Spc^r cassette, Fig EV1A), confirming the absence of the protein in the mutant strain by Western blot (Fig EV1B). Once *XccbphP* growth curves were confirmed to be similar to the wild-type strain (Fig EV3), we were prompted to evaluate the influence of *Xcc*BphP in bacterial virulence. For that purpose, 10-day-old *Arabidopsis* plant seedlings were inoculated with the bacterial strains cultures under normal laboratory conditions. After 1 or 3 days post-infection (d.p.i.), colony forming units (CFU) per plant milligram were determined. Our results show that at 3 d.p.i. the *XccbphP* strain exhibits a significantly more virulent phenotype, meaning a higher capacity to replicate inside the host, compared to the wild type (Fig 2A). Interestingly, the complemented strain (p*Xcc*BphP), which displays *Xcc*BphP overexpression (Fig EV1B), behaves as an attenuated strain showing lower CFU counts than the wild type after 3 d.p.i. (Fig 2A). We then sought to examine whether these differences in bacterial infection are dependent on light. Consequently, before plant inoculation, all bacterial strains were either cultured in the dark or under continuous white illumination. Plants infected with

wild-type and p*Xcc*BphP-complemented bacterial strains cultured in light displayed lower CFU counts at 2 d.p.i. compared to the cultures kept in the dark. *XccbphP* ability to infect plants remained comparable regardless of the light conditions, and always greater than the wild-type strain. Similarly, when plants were infected with the *XccbphP* mutant complemented with the photo-inactive *Xcc*BphP-C13S version (pC13S), no statistical differences were detected between light and dark conditions (Fig 2B).

The aerial part of terrestrial plants possesses microscopic pores called stomata, which allows the control of gas exchange (necessary for photosynthesis) and water loss. Plants regulate the opening and closing of stomata by different mechanisms [26]. It has been reported that *Xcc* is able to reverse both pathogen- and abscisic acid-induced stomatal closure in *Arabidopsis* through a virulence factor of a still unknown composition that is secreted to the extracellular medium [17]. To start elucidating the mechanisms by which *Xcc*BphP modulates plant infection, we studied the pathogen-induced stomatal closure as part of the plant innate immune response. In order to determine whether the increase in *XccbphP* virulence is related to its ability to penetrate into the host through stomata, we measured its capacity to promote stomatal closure in the light. Strikingly, stomata from epidermal peels incubated with *XccbphP* remained significantly opened at 1 h post-incubation (h.p.i.). As expected, the wild-type and complemented p*Xcc*BphP strains promoted normal stomatal closure. Stomata also remained opened when they were incubated with pC13S strain, although with lower amplitude compared to the *XccbphP* mutant (Fig 2C). Moreover, both wild-type and *XccbphP* strains promote stomata opening at 3 h.p.i by producing the yet unidentified compound (Fig EV4) [17]. Therefore, to evaluate a possible scenario in which the infection occurs in the dark (when stomata are closed) we assayed the capacity of *Xcc* strains to promote stomatal opening of dark-adapted stomata. Results show that wild-type *Xcc* is in fact able to open stomata at 3 h.p.i., while *XccbphP* shows an even better performance on this task (Fig 2D).

Previous reports suggest that xanthan specifically suppresses local plant defense by the inhibition of callose (a β-1, 3-linear glucan that strengthens plant cell walls) deposition, which is required for disease resistance against *Xcc* [27,28]. Consequently, we measured callose biosynthesis during *XccbphP* infection. Leaves were challenged with wild-type *Xcc*, *XccbphP*, p*Xcc*BphP, pC13S, and flg22 peptide, a 22-amino acid sequence of the conserved flagellin N-terminus that is known to activate the plant defense mechanisms [29]. Twenty-four hours after infection, the inoculated leaves were stained for callose with aniline blue and cytological observations were performed at the sites of infection with UV-fluorescence microscopy. Callose depositions can be identified as bright-blue points in leaves or veins (Fig 2E, top panel). The results indicate that *XccbphP* presents considerable reduced callose deposits compared to the wild type, the p*Xcc*BphP strain, and the flg22 peptide (Fig 2E, bottom panel). In turn, pC13S presents similar values to those of p*Xcc*BphP. These results are consistent with the results obtained in plant infection assays presented above.

*Xcc*BphP is involved in β-1, 4-endoglucanase production

We then focused on extracellular hydrolytic enzymes, which are virulence factors secreted by the type 2 secretion system (T2SS) that
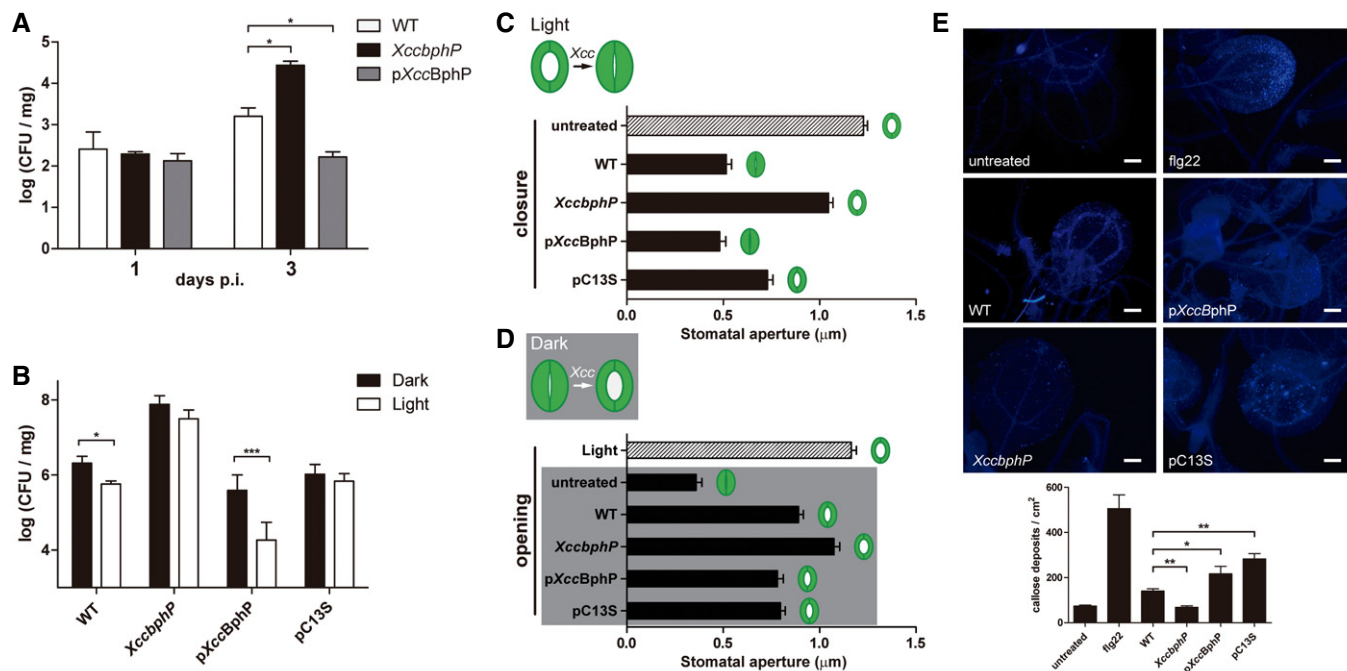
Figure 2. *Xcc*BphP functions as a negative regulator for *Xanthomonas campestris* infection affecting plant defenses.

A, B   *Arabidopsis thaliana* plants were inoculated with wild-type, *Xccbphp*, p*Xcc*BphP, or pC13S bacterial strains cultured prior to inoculation under (A) normal laboratory illumination or (B) under light or dark conditions. After 1, 2, or 3 d.p.i., CFU per plant mg were determined (n = 3 replicates). Data presented here derive from more than four independent experiments.

C, D   (C) Stomatal closure in the presence of bacterial strains or not (untreated) after 1 h under light conditions. (D) Stomatal opening after 3 h of incubation with bacterial strains or not (untreated) in the dark. A control treatment without bacteria and illuminated was included (Light). (C, D) Stomatal apertures were recorded (n = 80 replicates). Data are representative of two independent experiments.

E   *Arabidopsis thaliana* leaves were inoculated with wild-type, *Xccbphp*, p*Xcc*BphP, and pC13S strains, stained for callose deposits and observed by fluorescence microscopy. MgCl$_2$ buffer (untreated) and flg22 peptide were used as negative and positive controls, respectively. Top panel: representative pictures of three independent experiments. Scale bar represents 200 μm. Bottom panel: the number of callose deposits per field of view (0.45 mm^2) were determined (n = 8 replicates). Data are representative of two independent experiments.

Data information: (A–E) Values are expressed as mean ± s.e.m. Statistical analysis was performed by a two-tailed Mann–Whitney test (*P < 0.05, **P < 0.01, ***P < 0.001).

allow *Xcc* to degrade plant material and support infection [30]. A direct influence on the plant–pathogen interaction was demonstrated for a secreted endoglucanase enzyme from *Xcc* [31]. Endoglucanase activity from bacterial culture media can be estimated by measuring the degradation halo it produces in carboxymethyl cellulose (CMC) plates. Figure 3A shows that the overexpressing p*Xcc*BphP complemented strain displays significantly lower levels of endoglucanase activity compared to the wild type, although no light/dark regulation was detected. A quantitative colorimetric assay in solution was performed to measure β-1, 4-endoglucanase enzymatic units. Because we were not able to detect differences between the light/dark treatments before, we decided to perform the experiments under normal laboratory light conditions. CMC degradation plate assay results were corroborated in this system. Moreover, p*Xcc*BphP strain culture supernatants possess an almost 10-fold reduction in endoglucanase units compared to the wild type (Fig 3B).

*Xcc*BphP regulates xanthan production and biofilm formation

Light regulates the plant endosymbiont *R. leguminosarum* infectivity levels through a blue-light photoreceptor (LOV-HK) [3]. This regulation can be partially explained by the fact that exopolysaccharide (EPS) production and biofilm formation, intimately related to infection, are controlled by LOV-HK in a light-dependent manner [3]. Similarly, the EPS xanthan produced by *Xanthomonas* is a virulence factor and is involved in biofilm development. Disruption of xanthan production impairs *Xcc* biofilm development *in vitro* and bacterial virulence [32,33]. Hence, we sought to associate the low *Xcc* infectivity levels induced by light treatments (Fig 2B) with low EPS production and poor biofilm development. To evaluate EPS production, bacteria were plated in rich media, cultured under light or dark conditions continuously for 48 h and EPS production quantified as a measure of colony diameter. As shown in Fig 4A, wild-type *Xcc* produces significantly more EPS in the dark than in the light treatment. Interestingly, the *Xccbphp* mutant is insensitive to light or dark and produces significantly more xanthan in both conditions compared to the wild-type strain. In contrast, p*Xcc*BphP-complemented strain colonies exhibited a severe decrement in xanthan content in both dark and light, although maintaining the tendency of light regulation. The *Xccbphp* mutant was complemented with a gene coding for the photo-inactive *Xcc*BphP-C13S, which had no effect in restoring the wild-type phenotype (Fig 4A) although the protein was overexpressed, similarly to p*Xcc*BphP
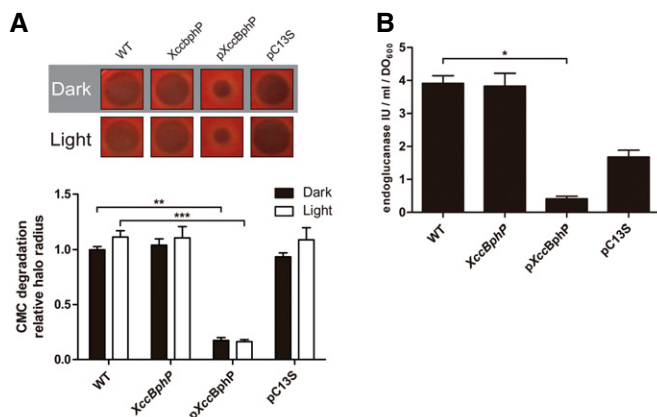
Figure 3. *Xanthomonas campestris* extracellular endoglucanase production is regulated by *Xcc*BphP.

A   Five microlitre supernatants from wild-type, *Xccbphp*, p*Xcc*BphP, and pC13 strains bacterial cultures (OD$_{600}$ = 1) grown under light or dark conditions were plated onto PYM-carboxymethyl cellulose (CMC) agar plates and revealed with Congo red staining (*n* = 2 replicates). The extracellular β-1,4-endoglucanase production levels correlated with CMC degradation halo radiuses (top panel). Halo measurements are presented in the bottom panel. Data derive from ten independent experiments.

B   The extracellular β-1,4-endoglucanase activity from bacterial cultures supernatants (OD$_{600}$ = 1) was determined by a colorimetric assay in solution (*n* = 2 replicates). Wild-type, *Xccbphp*, p*Xcc*BphP, and pC13 strains were assayed under normal laboratory conditions. Data derive from three independent experiments.

Data information: (A, B) Values are expressed as mean ± s.e.m. Statistical analysis was performed by a Kruskal–Wallis test and Dunn's multiple comparison test (*P < 0.05, **P < 0.01, ***P < 0.001).

(Fig EV1B). Xanthan content was also measured in liquid cultures confirming the results obtained in agar plates and evidencing that the only light-responsive strains are the wild type and the complemented strain bearing a wild-type copy of *XccbphP* (Fig 4B). Accordingly, when the sliding motility—a type of bacterial movement that depends on EPS, which reduces the friction between cells and substrate [34]—was assayed, it was observed that sliding in *XccbphP* was strongly enhanced while distinctly impaired in p*Xcc*BphP compared to the wild type. As expected, the pC13S strain cannot restore the wild-type phenotype and slides comparable to the *XccbphP* mutant (Fig EV5A).

The hypothesis that EPS regulation by light impacts on biofilm development was tested by confocal laser-scanning microscopy (CLSM) studies of *Xcc* biofilms cultured in chambers in the dark or under continuous white light without agitation. After 4 days, a clear impairment in the wild-type biofilm maturation in the light treatment was confirmed by the CLSM picture analysis while a completely mature biofilm is found to be formed in the dark condition (Fig 4C). In contrast, and reminiscent of the EPS experiments, the *XccbphP* and the pC13S strains were able to generate mature biofilms regardless of the light condition while the complemented strain exhibits its wild-type phenotype restored (Fig 4C). Consistently, a biofilm COMSTAT analysis revealed that wild-type and p*Xcc*BphP strains show increased values in biomass and average thickness in dark compared to the light treatment (Table EV2). Moreover, these variables are increased in *XccbphP* and pC13S in

both light and dark conditions compared to the wild type. These results are in agreement with *Xcc*BphP sensing light and lowering EPS levels, which in turn produces an immature biofilm.

Far-red light and *Xcc*BphP overexpression produce genomewide transcriptional changes

In order to find clues on the *Xcc*BphP signal transduction mechanism of the far-red light pathway at the transcriptional level, we performed RNA-Seq of the wild type cultured in the dark or under far-red light, and the *Xcc*BphP overexpressing strain p*Xcc*BhpP in far-red light. A principal component analysis (PCA) clearly shows that the biological replicates for each treatment cluster together but not the treatments themselves (Fig 5A). Hence, the transcriptomes from the treatments differ as if they were different "bacterial states". To find differentially expressed (DE) genes with statistical significance (P < 0.05), pairwise comparisons between treatments were performed. Strikingly, 1,121 DE genes were found to be caused by illumination alone. This represents 25.6% of the *Xcc* genome which codes for 4,381 identified ORFs. In addition, when the dark wild type was compared with illuminated p*Xcc*BphP, 1196 DE genes arose. Furthermore, these two comparisons share 882 DE genes. In contrast, when p*Xcc*BphP and wild-type far-red datasets were compared, 196 DE genes appeared, representing 4.47% of the total genomic ORFs (Fig 5B). There are 81 out of these 196 DE genes which are common to all three comparisons making this group of particular interest. There is another group of genes that do not change in the wild type upon illumination but indeed change when *Xcc*BphP is overexpressed containing 272 DE genes. This group is composed of two subgroups: 256 DE genes exclusively found in the wild-type dark/p*Xcc*BphP intersection and 16 DE genes that are exclusive in the intersection between the far-red irradiated strains. These genes are dependent on *Xcc*BphP levels and do not show statistical differences due to illumination in the wild type (Fig 5B).

A Gene Ontology (GO) analysis was performed to evaluate relative enrichment of GO terms in the three dataset comparisons. The three GO categories consist of biological process (BP), molecular function (MF), and cell compartment (CC). The datasets contained DE genes which correspond to GO terms with differential enrichment factors which can be inferred to be related to virulence and signal transduction in *Xcc* (Fig 5C). This analysis helped us visualized the GO terms of DE genes dependent on far-red light and *Xcc*BphP involved in many of the experiments performed during this work, which implicate: (i) secretory systems of hydrolytic enzymes, including endoglucanases and proteases, (ii) adhesion, motility, and xanthan metabolism, necessary for proper biofilm development, and (iii) cell signaling systems that might include components of the red-light-*Xcc*BphP downstream signaling (Fig 5C). A comprehensive list of DE selected genes that fall into these categories was elaborated, comprising many virulence factors and pathogenic-related systems (Dataset EV1).

Xcc*BphP downregulates transcription of virulence systems

Finally, we focused on those genes coding for reported *Xanthomonas* virulence effectors and studied along the present work. Particularly,
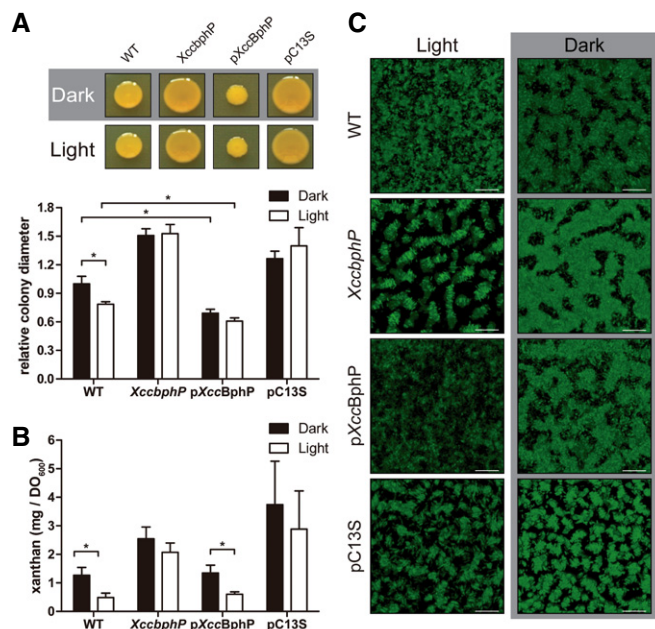
Figure 4. *Xanthomonas campestris* virulence factors are inhibited by light through *Xcc*BphP.

A   Five microlitres from wild-type, *Xccbph*P, p*Xcc*BphP, and pC13S bacterial cultures (OD_{600} = 1) were plated onto PYM-glucose agar plates under light or dark conditions. Xanthan production was determined measuring colony diameters (*n* = 4 replicates) for 20 independent experiments.

B   Wild-type, *Xccbph*P, p*Xcc*BphP, and pC13S were grown in 20 ml PYM liquid medium under light or dark conditions. Extracellular xanthan was purified by KCl addition and ethanol precipitation, then dried, and weighed (*n* = 2 replicates) for four independent experiments.

C   Representative confocal laser-scanning microscopy pictures of biofilm development of bacteria cultured for 4 days in minimal medium in chambered cover slides under light or dark conditions. The scale bar represents 30 µm.

Data information: (A, B) Values are expressed as mean ± s.e.m. Statistical analysis was performed by a Kruskal–Wallis test and Dunn's multiple comparison test (*$P < 0.05$).
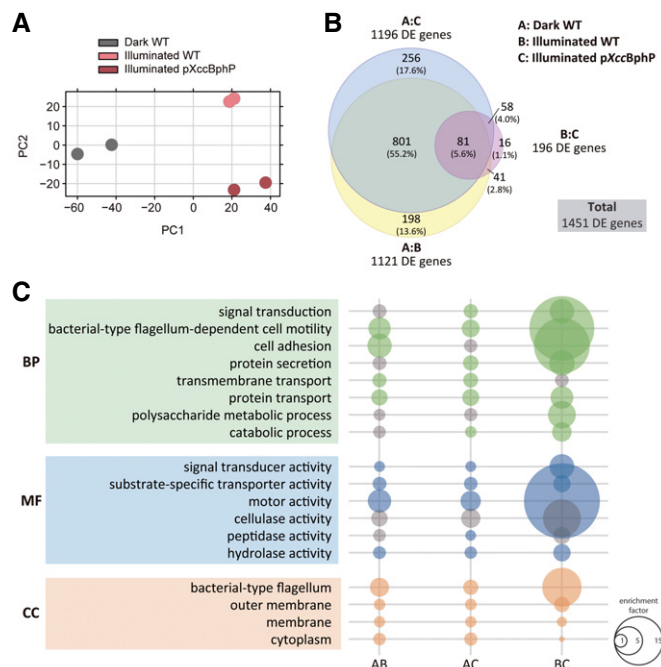

Figure 5.   Genomewide differential expression RNA-Seq analysis between treatments.

A   Principal component analysis (PCA) plot of the first two components of the analyzed samples showing separation between the three treatments: far-red illuminated wild-type, far-red illuminated p*Xcc*BphP (*Xcc*BphP overexpressing), and dark wild-type *Xcc* treatments.

B   Venn diagram showing overlap of differentially expressed (DE) genes between treatments (*P*-values < 0.05), bubbles are drawn to scale. A total of 1,451 DE genes were found in comparisons between all treatments and relative percentages to this number are indicated.

C   Gene Ontology (GO) enrichment analysis. GO enrichment was evaluated at three different levels: biological processes (BP), molecular function (MF), and cellular component (CC). Relevant categories showing enrichment of DE genes are depicted. Bubble size correlates with enrichment factor values; gray bubbles represent *P*-values > 0.05.

DE genes involved in extracellular endoglucanase activity, xanthan production, and motility were selected. The first group of genes that caught our attention were the endoglucanases and the T2SS (*xps*), involved in exporting degradative enzymes outside the cell [31,35]. Most endoglucanase and all *xps* T2SS DE genes are downregulated in p*Xcc*BphP compared to wild type cultured under any condition (Dataset EV1). This finding is consistent with the results shown in Fig 3. The second group of genes found to be *Xcc*BphP-dependent is gathered in the *gum* operon, responsible for xanthan gum production [32]. Again, we observed that p*Xcc*BphP strain shows statistically lower transcriptional levels of *gum* genes than the wild type (Dataset EV1), which may explain why this strain produces significant less xanthan in the plate assay than the wild type (Fig 4A). Flagellar genes (*flg* and *fli*) constitute the third group of selected DE genes, which are known to be necessary for *Xanthomonas* virulence [34]. They exhibit a strong downregulation with *Xcc*BphP overexpression (Dataset EV1), suggesting an impairment in flagellar-dependent motility for p*Xcc*BphP strain. Concordantly, our results clearly show that p*Xcc*BphP is indeed diminished in swimming motility (Fig EV5B).

Discussion

Bacteria inhabit all of our planet ecosystems, including the phyllosphere, the aerial parts of the plants, which is considered a hostile environment for the colonists. Bacteria are the most abundant members of the phyllosphere community and have been shown to colonize leaves at densities of up to 10^8 cells per cm^2 [36]. During the day, bacteria are exposed to high visible light intensities and UV-B radiation levels that can damage their metabolism and physiological processes [37,38]. Phytopathogenic bacteria living in the leaves take advantage of specific adaptations that allow them to survive and infect their hosts [18]. However, there is still little information on how they respond to environmental light. Recent reports have shown that photoreceptors are involved in virulence and motility of different *Pseudomonas syringae* pathovars, suggesting that light is important for their pathogenicity [13,39–41]. *Xcc* is adapted to the phyllosphere environment, but so far there is a lack of knowledge on the role of light in its physiology, which stimulated us for the present study.
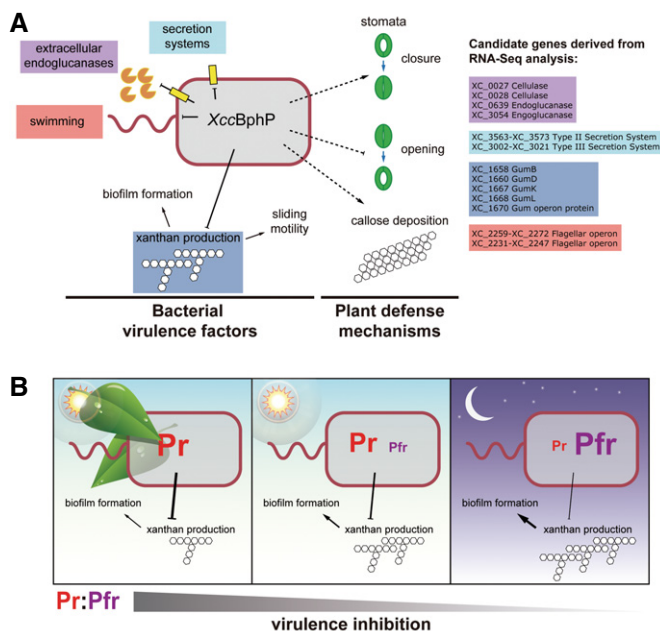
A

B

Figure 6. *Xcc*BphP functions as a negative regulator for virulence through transcriptional regulation.

A   Scheme derived from the results obtained throughout this work from the wild-type, the *XccbphP* (null mutant), and the complemented p*Xcc*BphP (overexpressing) strains. Systems affected are indicated in different colors, and gene candidates involved in these systems found by RNA-Seq analysis that are regulated by *Xcc*BphP are depicted in the same color code.

B   Possible model for *Xcc*BphP light-regulated EPS and biofilm results integrated with the spectroscopic data. *Xcc*BphP downregulates biofilm formation, xanthan production, and consequently *Xcc* virulence in a Pr:Pfr-dependent manner. *Xcc*BphP exposed to sunlight filtered by a canopy (left), direct sunlight (middle), or darkness (right).

Our data demonstrate that *Xcc*BphP is a functional bathy-type bacteriophytochrome *in vitro* as well as *in vivo*. We could establish *in vitro* that *Xcc*BphP can be photoconverted between the Pr and Pfr forms, the Pr/Pfr equilibrium ratio depends on the quality of sunlight, and that these light-induced changes are dependent on the presence of the conserved Cys13 residue. Moreover, the absence of *Xcc*BphP *in vivo* boosts *Xcc* virulence likely by (i) an increment in many bacterial virulence factors and (ii) its ability to bypass the plant defense mechanism. In this sense, the excessive production of xanthan was discarded as a possible explanation for the *Xcc*BphP mutant strain not triggering stomatal closure as the *gumB* mutant, unable to produce xanthan, behaves similar to the wild-type strain in stomatal closure experiments (Fig EV4). On the other hand, *Xcc*BphP overexpression attenuates virulence, likely through transcriptional downregulation of virulence factors as revealed by our RNA-Seq results. These findings were gathered and summarized in Fig 6A.

Moreover, *Xcc* is significantly less virulent in the light than in the dark and this is dependent on *Xcc*BphP. Taking together virulence, xanthan EPS, biofilm, and spectroscopy experiments, a simple hypothetical model can be envisaged for *Xcc* light/dark virulent behavior, which is consistent with light inhibition of xanthan production and biofilm maturation, probably triggered by a low Pfr:Pr ratio

(Fig 6B). Hence, *Xcc*BphP may be described as a virulence negative regulator, which senses light and partially inhibits the *Xcc* virulence program.

Why a bacteriophytochrome photoreceptor downregulates virulence toward its host is an open question. It is possible that *Xcc* is constitutively primed for infection and as the light stimuli disappear, it can promptly respond by increasing its virulent behavior. Consistently, *Xcc* rapidly establishes infection in a period significantly shorter than a daily photoperiod. Another reason for virulence inhibition could be attributed to *Xcc* hemibiotrophic lifestyle [31], initially infecting live tissues and at later stages actively killing host cells during its life cycle, and an excess in its pathogenicity toward its host could result non-adaptive. Therefore, *Xcc*BphP might have evolved to control and fine-tune *Xcc* virulence by inhibiting it. It is worth mentioning that *Xcc* can also (i) survive in the soil independently from its host for several weeks and (ii) produce a seedborne disease [16]. In this scenario, photoreception can also be playing a part in signaling (time or place) the bacteria for infection in its life cycle, similarly to *Brucella* or *Rhizobium* [3,4]. One possibility is that *Xcc*BphP serves as a time signaling system to distinguish between day and night. In line with this, it is known that light impacts positively on the plant immune system, probably making daytime the less favorable moment for infection. Plant defense mechanisms are modulated by light and circadian rhythm involving phytochrome photoreceptor signaling, among others [42,43]. In *Arabidopsis*, plant defense responses and disease resistance significantly depend on the time of day; morning or midday infections result in a more pronounced hypersensitive response than evening or night infections [44]. Moreover, light is also associated with the production of ROS that in turn act in the plant–pathogen interaction [45]. In this sense, it is reasonable to think that *Xcc* can synchronize infectivity to the plant dark-susceptible period by means of its BphP. Synchronizing *Xcc* infectivity to an optimal moment of the host physiology and signaled by light/dark as environmental cues can be a feature shared by other infective bacteria that harbor photoreceptors. In an analogous fashion, the quorum-sensing (QS) systems that are present in *Xcc* and in many other pathogenic bacteria, activates infection when the bacteria reach an appropriate situation (i.e. a certain population density) [46,47]. Another possibility is that *Xcc*BphP signals for a spatial cue. During the day, within a leaf canopy, most red light has been removed by the chlorophyll in shading leaves but almost none of the far-red light [48]. Hence, the light environment within the canopy may largely drive *Xcc*BphP from a Pfr to a Pr form, as observed in Fig 1D, decreasing *Xcc* virulence levels relative to direct sunlight exposure. Therefore, there should also be differential *Xcc* virulence during daytime in shaded and non-shaded tissues. In this manner, *Xcc* might be optimizing its virulence levels (i.e. resources) according to the tissues susceptibilities as shaded leaves are more susceptible to infections that those ones that are exposed to direct light [42].

The *Xcc*BphP red-light-signaling pathway remains to be elucidated. It is plausible that the *Xcc*BphP first transducing events are transmitted to downstream elements via protein–protein interactions through the PAS9 output module [23]. Our group has recently published a crystallographic structure of the full-length *Xcc*BphP in the Pr state (PDB code 5AKP), revealing a parallel dimer arrangement with its complete PAS9 module, that may serve as starting

material for studies on early signaling events for this photoreceptor [22]. Moreover, the RNA-Seq results show that there is a massive rearrangement of putative genes involved in this pathway, comprising (i) histidine kinases, (ii) two-component systems, (iii) c-di-GMP-modulating enzymes, and (iv) transcriptional regulators, all of which change due to far-red illumination and/or *Xcc*BphP overexpression (Dataset EV1). To conclude, our findings strongly suggest that light is an important environmental cue sensed by *Xcc*BphP that regulates virulence-associated mechanisms, which ultimately govern the plant–microbe interactions in *Xcc*. The understanding of *Xanthomonas* photobiology and its relationship with virulence may help in the task of finding novel ways to interfere with its infection cycle.

Materials and Methods

Bacterial strains and culture conditions

Xanthomonas campestris pv. *campestris* 8004 (*Xcc*) strains were cultured in PYM or in Y minimal medium (YMM) [49,50] at 28°C, with agitation (250 r.p.m.). To examine biofilm development, bacteria were grown in YMM containing 1% (wt/vol) glucose as the carbon source [51]. *Escherichia coli* strains were cultured at 37°C in Luria-Bertani medium. When required, the antibiotics rifampicin (Rif), kanamycin (Km), spectinomycin (Spc), chloramphenicol (Cm), and ampicillin (Amp) were added in final concentrations of 30, 35, 100, 20, and 100 μg/ml, respectively.

A complete list of strains, plasmids, and primers used in this study is included in Table 1.

Light, far-red, and dark bacterial culture conditions

Light treatments were performed with continuous white light (2,700 K) from fluorescent tubes with a fluence of 15 μmol/m/s. Photon flux was measured using a Quantum Meter (Apogee Instruments model QMSW-SS). Far-red bacterial illumination was performed using 733 nm 0.7 W LEDs at a 15 cm distance during culture. Darkness was achieved covering cultures with two layers of aluminum foil.

Generation of the bacterial strains

The *XccbphP* mutant strain was obtained by allelic exchange. The *XccbphP* gene (XC_4241) was partially deleted and replaced by a 2 kb Sm^r/Spc^r cassette (Ω) [52]. Two fragments from the flanking regions of *XccbphP* gene were amplified using primers ΔBphP_A-ΔBphP_B and ΔBphP_C-ΔBphP_D, respectively. The fragments were BamHI-digested, ligated to each other, amplified using the ΔBphP_A-ΔBphP_D primers, and the product cloned into the pGEM-T Easy vector (Promega). The resulting vector was BamHI-digested, blunted with Klenow Fragment (New England Biolabs) and ligated to a SmaI-digested Ω cassette, derived from the pHP45Ω plasmid, to yield pG-*XccbphP*::Ω. The *XccbphP*::Ω construction was subcloned into pk18mobsacB [53] in the HindIII restriction site. The resulting pK-*XccbphP*::Ω vector was used to transform *Xcc*. Sucrose-resistant double recombinants were selected (Km^s, Spc^r). The mutation was confirmed by PCR sequencing, using specific primers

(5_Flank_F-3_Flank_R) flanking the mutation site and by Western blot. To construct the *XccbphP* complemented strain, a 2.7-kb fragment containing the complete XC_4242-XC_4241 operon and its regulatory sequences was amplified using specific primers (cBphP_F and cBphP_R), cloned into the HindIII restriction site of pBBR1MCS2 vector [54], to yield pBBR-*Xcc*BphP, which was used to transform *XccbphP* to generate p*Xcc*BphP strain. The *Xcc*BphP-C13S complemented strain was generated by site-directed mutagenesis using Q5 High-Fidelity DNA Polymerase (New England Biolabs), specific primers (C13S_F and C13_R) and the pBBR-*Xcc*BphP vector as template to generate the pBBR-C13S vector, which was used to transform *XccbphP* to generate pC13S strain.

Western blot

Bacterial extracts normalized by OD_{600} were loaded and separated in 12.5% SDS–PAGE electrophoresis. Similar amounts of protein were loaded into each lane of the gels, corroborated by Coomassie blue staining. Proteins were transferred to Immobilon-P PVDF Membrane (Millipore). Membranes were blocked with non-fat milk in PBS and incubated with an anti-*Xcc*BphP polyclonal antibody (1:1,000) and then with anti-mouse IgG (Fc specific)-peroxidase antibody produced in goat (Sigma) (1:5,000). Detection was achieved using the Amersham ECL Prime Western Blotting Detection Reagent (GE Healthcare Life Sciences) on an ImageQuant LAS 400 apparatus (GE Healthcare Life Sciences).

RT–PCR of *XccbphO-XccbphP* operon

Total *Xcc* bacterial RNA was isolated using the MasterPure™ RNA Purification Kit (Epicentre, Illumina). Reverse transcription was performed with a first-strand SuperScript III cDNA kit (Invitrogen), using random decamer primers (Invitrogen) and RNasin ribonuclease inhibitor (Promega). The Primer-BLAST program (http://www.ncbi.nlm.nih.gov/tools/primer-blast/) was used to design primers for PCR products of 100–125 bp (Table 1). The cDNA samples were used as templates in PCR amplification, and products were resolved in a 2% agarose gel.

Bioinformatics

BphP homologs were retrieved from UniProtKB database (2016_01 release) by means of a BLAST search in the UniProt server (http://www.uniprot.org/) using default parameters and the photosensory module (PAS2-GAF-PHY) from *Xcc*BphP as query. All sequences were inspected using Pfam server (http://pfam.xfam.org/). A total of 75 sequences from *Xanthomonas* genus containing a complete PAS2-GAF-PHY domain triad were identified. PHY domain sequences inferred by Pfam from this dataset were used to build a multiple sequence alignment using MUSCLE program and conducted in MEGA7 software [55]. Then, a molecular phylogenetic analysis by maximum-likelihood method was performed to obtain a tree. The evolutionary history was inferred by using the maximum-likelihood method based on the Whelan and Goldman model [56]. The tree with the highest log-likelihood (−1,872.6517) is shown. The percentage of trees in which the associated taxa clustered together is shown next to the branches. Initial tree(s) for the heuristic search were obtained automatically by applying Neighbor-Join and BioNJ

Table 1. Strains, plasmids, and oligonucleotides used in this study.

Strains	Genotype/relevant characteristics	Source
Xcc	*Xanthomonas campestris* pv. *campestris* 8004, Rif[r]	Laboratory stock
XccbphP	*Xcc*, XC_4241::Ω, Rif[r], Spc[r]	This work
pXccBphP	*XccbphP* + pBBR-*Xcc*BphP, Rif[r], Spc[r], Km[r]	This work
pC13S	*XccbphP* + pBBR-C13S, Rif[r], Km[r]	This work
gumB	*gumB*::Tn5lac, EPS minus, Rif[r], Km[r]	[28]
DH5α	*Escherichia coli*, *hsdR recA lac*ZYA *Φ*80 *lac*ZDM15	Gibco-BRL
BL21(DE3)pLysE	*Escherichia coli*, high-efficiency protein expression strain	Promega
pET-*Xcc*bphP	BL21(DE3)pLysE, pET-*Xcc*bphP, Cm[r], Km[r]	This work
pET-C13S	BL21(DE3)pLysE, pET-C13S, Cm[r], Km[r]	This work
Plasmids	**Relevant characteristics**	**Source**
pGEM-T Easy	PCR cloning vector, *lacZ*, Amp[r],	Promega
pG-*XccbphP*::Ω	pGEM-T Easy with Ω cassette (*aadA* gene) cloned between a 400-bp and a 500-bp fragments flanking *XccbphP* gene, Amp[r], Spc[r]	This work
pKmobSacB	Suicide vector, *sacB mob lacZ*, Km[r]	[53]
pK-*XccbphP*::Ω	pKmobsacB with *XccbphP*::Ω construction, Km[r], Spc[r]	This work
pBBR1MCS2	Broad-host-range cloning vector, Km[r]	[54]
pBBR-*Xcc*BphP	pBBR1MCS2 with a 2,708-bp fragment containing *XccbphO-XccbphP* operon and 5′ regulatory sequence cloned in HindIII site, Km[r]	This work
pBBR-C13S	Originated from pBBR-*Xcc*BphP, containing mutation coding for *Xcc*BphP C13S, Km[r]	This work
pET-*Xcc*BphP	pET24a, Hisx6-Full-length *Xcc*BphP, Km[r]	This work
pET-C13S	pET24a, Hisx6-Full-length *Xcc*BphP-C13S, Km[r]	This work
Oligonucleotides	**Sequence (5′ − 3′)**	**Source**
ΔBphP_A	CTAAGCTTTACCTACGCGCAGGTGCTGCGCCGGCATC	This work
ΔBphP_B	ATGGATCCCGCGCGCAGACGTCCAGGTCCAACGGGTTG	This work
ΔBphP_C	TTGGATCCGCCGTTGCAAGTGAGCGACGGCGCACCGG	This work
ΔBphP_D	TCAAGCTTACGCTGCGCCTGTGCCGCAAGGCCGCTGC	This work
cBpbP_F	CTAAGCTTTGGCGCGCCGCTGCACCTGCCC	This work
cBpbP_R	TTCAAGCTTCTCTTATTCCGGATCGCGCAGCTGTAAC	This work
5_Flank_F	GTGCCGCTGATGCAGGCGCTGGGGCAGG	This work
3_Flank_R	GCAAGGCGATCAAGGTGATCGCACCGG	This work
C13S_F	TTGGACCTGGACGTCTCCGCGCGCGAACCCATC	This work
C13S_R	GATGGGTTCGCGCGCGGAGACGTCCAGGTCCAA	This work
BphP_F	ATCATATGCACCATCACCATCACCATAGCACTGCAACCAACCCGTTG	This work
BphP_R	TAGGATCCTTATTCCGGATCGCGCAGCTGTAAC	This work
RT_1	CCCGGGTTGAGTCGGTGC	This work
RT_2	GCCAGCAGCCGGTGATGC	This work
RT_3	AGCAACGCCTGCAGAGCG	This work
RT_4	CCAACGGGTTGGTTGCAGTG	This work
RT_5	GCCAGTTCCACCTTGAACCTCT	This work
RT_6	GCAGTCATTTTGATCGCTGCTC	This work

algorithms to a matrix of pairwise distances estimated using a JTT model, and then selecting the topology with superior log-likelihood value. A discrete Gamma distribution was used to model evolutionary rate differences among sites [five categories (+G, parameter = 3.3628)]. All positions containing gaps and missing data were eliminated. There were a total of 144 positions in the final

dataset. The resulting tree was plotted using iTOL server (http://itol.embl.de/) [57].

Generation and purification of *Xcc*BphP and *Xcc*BphP C13S recombinant proteins

Full-length *Xcc*BphP (residues 1–634) was cloned from the XC_4241 ORF into the NdeI/BamHI restriction sites of the pET24A vector (Novagen) to generate pET-*Xcc*BphP as described elsewhere [58]. The *Xcc*BphP-C13S point mutant was generated by site-directed mutagenesis using Q5 High-Fidelity DNA Polymerase, specific primers (C13S_F and C13_R) and the pET-*Xcc*BphP vector as template to generate the pET-C13S vector. *Escherichia coli* BL21(DE3)pLysE strain cells were transformed with pET-C13S. Cultures were induced with a final concentration of 0.4 mM IPTG overnight at 20°C with agitation (250 rpm), cells were harvested and ruptured. Next, the His-tagged proteins were purified as previously described [58]. The holoproteins were generated by incubating the apoproteins for 1 h at room temperature in the presence of biliverdin-IXα (BV; Sigma-Aldrich) before the size-exclusion chromatography step. Protein concentration was estimated using the calculated molar extinction coefficient at $\lambda = 280$ nm provided by the ExPASy ProtParam tool (http://web.expasy.org/protparam/) based on the polypeptide sequence for the monomer ($\varepsilon_{XccBphP} = \varepsilon_{C13S} = 74,370$ M/cm); the biliverdin cofactor contribution was subtracted.

UV-vis spectroscopy

Quartz cuvette containing holoprotein 1 mg/ml solutions of *Xcc*BphP or C13S in 50 mM Tris–HCl pH 7.7, 250 mM NaCl (buffer A) was irradiated for 10 min with a white (2,700 K) 15-W fluorescent tube lamp, a red (630 nm) 1-W LED, far-red (733 nm) 0.7-W LED, direct sunlight or sunlight filtered with two layers of fresh green *Epipremnum aureum* leaves. Absorption spectra were collected in an 8452A diode array spectrometer (Hewlett Packard). The dark states were determined after proteins were kept in the dark for 96 h.

Plant materials

Arabidopsis thaliana (L.) Heynh. ecotype Col-0 seeds used for infection, callose staining, and stomatal aperture assays were surface sterilized with an ethanol:50%bleach:water (8:1:1) mixture for 5 min and rinsed three times with ethanol. Sterilized seeds were kept in water and in the dark for 3 days at 4°C. Seeds were germinated and cultivated in 60×15 cm Petri dishes containing Murashige and Skoog medium (MS), sucrose 0.5% and 0.5 g/l MES hydrate pH 5.7. Plants were grown at 22–23°C with a 12-h photoperiod for 10 days.

Infection assays

Bacterial strains were grown overnight in PYM supplemented with the appropriate antibiotics and resuspended in water. Plants were infected adding the bacterial suspension to the plant growth medium to a final OD_{600} of 0.002, as previously described [28]. Plants were kept at 22–23°C with a 12-h photoperiod. Daily samples were taken for 3 days. Bacterial content was determined by plating

a dilution series on PYM medium containing appropriate antibiotics of the homogenate leaves, and were expressed as CFU per gram of plant fresh weight.

Stomatal assays

Stomatal experiments were performed as previously described [17]. Briefly, for stomatal closure assays, epidermal peels from 4-week-old leaves were floated in 10:10 buffer (10 mM KCl and 10 mM MES-KOH pH 6.15) under light for 2 h, then 10^8 CFU/ml of each bacteria strain, flg22 peptide (5 μM, GL Biochem) or abscisic acid (20 μM, mixed isomers Sigma) were added to the medium and incubated for 1 or 3 h. Similarly, for stomatal opening assays, epidermal peels were incubated in buffer 10:10 for 2 h in the dark, then 10^8 CFU/ml of each bacterial strain were added to the medium and incubated for 3 h.

Apertures from 80 stomata for each experiment were measured in a Carl Zeiss microscope (4003) with the aid of an eyepiece micrometer.

Callose staining

Experiments were performed as described previously [29]. Briefly, following treatment with bacteria (5×10^8 CFU/ml) or flg22 peptide (100 nM, GL Biochem), 10-day-old seedlings grown in 12-well microtiter dishes were fixed in a 3:1 ethanol:acetic acid solution for several hours. The fixative was changed several times to ensure both thorough fixing and clearing of the tissues, which is essential for good callose detection. Seedlings were rehydrated in 70% (vol/vol) ethanol for 2 h, 50% ethanol for an additional 2 h, and water overnight. After three water washes, seedlings were treated with 10% (wt/vol) NaOH and placed at 37°C for 1–2 h to make the tissues transparent. After four water washes, seedlings were incubated in 150 mM K_2HPO_4 pH 9.5, and 0.01% (wt/vol) aniline blue (Sigma-Aldrich) for several hours. Seedlings were mounted on slides, and callose was observed using a Nikon Eclipse E600 fluorescence microscope (excitation $\lambda = 390$ nm; emission $\lambda = 460$ nm).

Xanthan production: agar plate assay

Xanthan production was determined measuring the diameter of the colonies grown in PYM supplemented with 2% (wt/vol) glucose. Five microliters of bacterial cultures ($OD_{600} = 1$) for each strain was inoculated in the plates and cultured under light or dark conditions for 48 h. Colony diameters were determined analyzing plate pictures using the ImageJ 1.41 software.

Xanthan production: liquid culture assay

Xanthan quantification in liquid culture was performed as described before [59]. Briefly, strains were cultured under light or dark conditions for 48 h at 28°C in 20 ml PYM liquid medium in 50-ml flasks, using an orbital shaker rotating at 200 rpm. Then, OD_{600} were recorded, cells removed by centrifugation (25,000 *g* for 60 min), the supernatants supplemented with KCl at 1% (wt/vol) final concentration, and 40 ml of ethanol were added. The precipitated crude xanthan was collected, dried, and weighed.

In vitro analysis of biofilm formation by confocal laser-scanning microscopy

Bacterial strains were cultured at 28°C in PYM medium supplemented with the proper antibiotics. Cultures were normalized by OD_{600} and diluted 1:2,000 in YMM and grown in coverglass slide chambers (no. 155411; Lab-Tek, Nunc) for 4 days at 28°C as previously described [60], under light or dark conditions. Cells were stained with LIVE/DEAD cell viability assay (Thermo Fisher Scientific Inc.) before visualization. Biofilm formation was monitored with an Olympus Fluo View 1000 confocal laser-scanning microscope (CLSM). Three-dimensional images were generated with the ImageJ 1.41 CLSM software from the National Institutes of Health (http://rsbweb.nih.gov/ij/download.html). COMSTAT software was used for three-dimensional biofilm structure quantifications [61].

CMC degradation halo assay

Production of extracellular β-1,4-endoglucanases was assessed inoculating 5 μl of supernatants onto PYM plates containing 0.125% (wt/vol) carboxymethyl cellulose (CMC, Sigma-Aldrich). Supernatants were obtained by centrifugation of 1 ml of bacterial cultures ($OD_{600} = 1$) for 5 min at 12,400 *g* that were grown under light or dark conditions. The CMC degradation halo was developed after 24 h of incubation with an aqueous solution 0.1% (wt/vol) Congo red (Sigma-Aldrich). Halo diameters were measured using the ImageJ 1.41 software. Data were normalized to the total area of the plate.

β-1,4-endoglucanase enzymatic activity: colorimetric assay in solution

The extracellular endoglucanase enzymatic activity measurements from liquid culture supernatants were performed by the colorimetric assay described before [62]. Briefly, bacteria were culture for 24 h at 28°C in 5 ml PYM liquid medium. Then, bacterial cultures OD_{600} were recorded, 1 ml of culture was centrifuged for 10 min at 9,000 rpm, and supernatants were used for a following reaction. A total of 50 μl of a supernatant dilution and 50 μl 2% CMC (wt/vol) both prepared in 0.05 M citrate buffer pH 4.8 were transferred to a 96-well plate, and the enzymatic reactions were incubated at 50°C for 60 min. The reducing sugar was measured by adding 100 μl of DNS (3,5-dinitrosalicylic acid), followed by an incubation of the mix for 5 min at 95°C, and the absorbance was measured at 540 nm. The enzymatic units were calculated as CMC (units/ml) = 0.185 (units/ml)/(enzyme concentration) to release 0.5 mg glucose, where concentration = (vol. enzyme in dilution)/(total dilution volume). All the results were normalized by OD_{600}.

Sliding motility assay

Bacteria were grown overnight in PYM medium; then, 3 μl of bacterial cultures ($OD_{600} = 1$) was inoculated in 0.5% (wt/vol) agar PYM plates as described before [34]. After 72 h, motility was assessed measuring the circular halo formed by the growing bacterial cells. The assay was performed in triplicates.

Swimming motility assay

Swimming motility assays were carried out as previously described [51]. Briefly, bacteria were grown overnight in PYM medium and 3 μl of bacterial cultures, normalized by OD_{600}, was used to inoculate NYGB medium [0.5% (wt/vol) peptone extract, 0.3% (wt/vol) yeast extract, 2% (vol/vol) glycerol] 0.25% (wt/vol) agar plates. After 72 h, motility was assessed by measuring the outer colony halo. The assay was performed in triplicates.

RNA isolation and RNA-Seq

Wild-type *Xcc* or p*Xcc*BphP strains were cultured in red light or dark conditions up to logarithmic phase (0.7–0.8 OD_{600}) at 28°C in PYM broth. Total bacterial RNA was isolated using the MasterPure™ RNA Purification Kit (Epicentre, Illumina). Samples corresponding to two biological replicates for each condition were submitted to Genome Québec for rRNA removal with Ribo-Zero (Illumina) and TruSeq RNA-seq library preparation. Fifty-basepair single-end sequencing of the libraries was performed using an Illumina HiSeq 2000 platform (Genome Québec). Removal of low-quality reads and Illumina adapters, and assessment of the quality of the reads was performed using Trimmomatic [63] and FastQC (http://www.bioinformatics.babraham.ac.uk/projects/fastqc/), respectively. Reads were aligned to the *Xcc* genome obtained from GenBank (accession number: NC_007086.1) using SAMtools and the Burrows-Wheeler Alignment software (BWA) [64,65]. Alignments were visualized using the software Integrated Genome Viewer (IGV) (http://broadinstitute.org/igv).

Gene annotation and RNA-Seq differential expression analysis

Open reading frames (ORF) were primarily annotated using the GenBank NC_007086.1 "locus_tag" accession number. For subsequent functional analysis, each ORF entry was then mapped to the following fields: (i) from GenBank NC_007086.1: "old_locus_tag" and "product", and (ii) from UniProtKB: "Protein names", "EC number", "Gene ontology (biological process)", "Gene ontology (molecular function)", "Gene ontology (cellular component)", and "Gene ontology IDs".

Read counts corresponding to annotated ORFs were quantified with the software FeatureCounts [66] using the strand-specific mode. Differential expression analysis was performed using the software DESeq [67]. Genes displaying adjusted *P*-value < 0.05 and baseline read counts higher than the first quartile of baseMean were informed as differentially expressed genes.

Gene ontology analysis

Using GO.db Bioconductor annotation data package in R language, all Gene Ontology (GO) terms and ancestors were retrieved and annotated for all *Xcc* ORFs. For differentially expressed (DE) genes, an enrichment test was performed for the following categories: BP (biological process), MF (molecular function), and CC (cellular component). The enrichment factor (EF) was estimated as the ratio between the proportions of genes associated with a particular GO category present in the dataset under analysis, relative to the proportion of the number of genes in this category in the whole genome. *P*-values were calculated using the Fisher's exact test.

Author contributions

HRB and FM wrote the manuscript; HRB, FAG, AAV, and FM conceived and designed the experiments; HRB, LT, GS, and FM performed the experiments; HRB, LT, RS, AMT, GEG, FCL, and FM analyzed data.

Conflict of interest

The authors declare that they have no conflict of interest.

References

1. Auldridge ME, Forest KT (2011) Bacterial phytochromes: more than meets the light. *Crit Rev Biochem Mol Biol* 46: 67 – 88

2. Purcell EB, Crosson S (2008) Photoregulation in prokaryotes. *Curr Opin Microbiol* 11: 168 – 178

3. Bonomi HR, Posadas DM, Paris G, Carrica Mdel C, Frederickson M, Pietrasanta LI, Bogomolni RA, Zorreguieta A, Goldbaum FA (2012) Light regulates attachment, exopolysaccharide production, and nodulation in *Rhizobium leguminosarum* through a LOV-histidine kinase photoreceptor. *Proc Natl Acad Sci USA* 109: 12135 – 12140

4. Swartz TE, Tseng TS, Frederickson MA, Paris G, Comerci DJ, Rajashekara G, Kim JG, Mudgett MB, Splitter GA, Ugalde RA *et al* (2007) Blue-light-activated histidine kinases: two-component sensors in bacteria. *Science* 317: 1090 – 1093

5. Kraiselburd I, Alet AI, Tondo ML, Petrocelli S, Daurelio LD, Monzon J, Ruiz OA, Losi A, Orellano EG (2012) A LOV protein modulates the physiological attributes of *Xanthomonas axonopodis* pv. citri relevant for host plant colonization. *PLoS ONE* 7: e38226

6. Rockwell NC, Lagarias JC (2010) A brief history of phytochromes. *Chemphyschem* 11: 1172 – 1180

7. Rockwell NC, Duanmu D, Martin SS, Bachy C, Price DC, Bhattacharya D, Worden AZ, Lagarias JC (2014) Eukaryotic algal phytochromes span the visible spectrum. *Proc Natl Acad Sci USA* 111: 3871 – 3876

8. Rockwell NC, Su YS, Lagarias JC (2006) Phytochrome structure and signaling mechanisms. *Annu Rev Plant Biol* 57: 837 – 858

9. Possart A, Fleck C, Hiltbrunner A (2014) Shedding (far-red) light on phytochrome mechanisms and responses in land plants. *Plant Sci* 217 – 218: 36 – 46

10. Hughes J (2013) Phytochrome cytoplasmic signaling. *Annu Rev Plant Biol* 64: 377 – 402

11. Hughes J, Lamparter T, Mittmann F, Hartmann E, Gartner W, Wilde A, Borner T (1997) A prokaryotic phytochrome. *Nature* 386: 663

12. Yeh KC, Wu SH, Murphy JT, Lagarias JC (1997) A cyanobacterial phytochrome two-component light sensory system. *Science* 277: 1505 – 1508

13. Wu L, McGrane RS, Beattie GA (2013) Light regulation of swarming motility in *Pseudomonas syringae* integrates signaling pathways mediated by a bacteriophytochrome and a LOV protein. *mBio* 4: e00334-13

14. Davis SJ, Vener AV, Vierstra RD (1999) Bacteriophytochromes: phytochrome-like photoreceptors from nonphotosynthetic eubacteria. *Science* 286: 2517 – 2520

15. Williams PH (1980) Black rot: a continuing threat to world crucifers. *Plant Dis* 64: 736 – 742

16. Vicente JG, Holub EB (2013) *Xanthomonas campestris* pv. *campestris* (cause of black rot of crucifers) in the genomic era is still a worldwide threat to brassica crops. *Mol Plant Pathol* 14: 2 – 18

17. Gudesblat GE, Torres PS, Vojnov AA (2009) *Xanthomonas campestris* overcomes *Arabidopsis* stomatal innate immunity through a DSF cell-to-cell signal-regulated virulence factor. *Plant Physiol* 149: 1017 – 1027

18. Vorholt JA (2012) Microbial life in the phyllosphere. *Nat Rev Microbiol* 10: 828 – 840

19. Bhoo SH, Davis SJ, Walker J, Karniol B, Vierstra RD (2001) Bacteriophytochromes are photochromic histidine kinases using a biliverdin chromophore. *Nature* 414: 776 – 779

20. Finn RD, Bateman A, Clements J, Coggill P, Eberhardt RY, Eddy SR, Heger A, Hetherington K, Holm L, Mistry J *et al* (2014) Pfam: the protein families database. *Nucleic Acids Res* 42: D222 – D230

21. Lamparter T, Carrascal M, Michael N, Martinez E, Rottwinkel G, Abian J (2004) The biliverdin chromophore binds covalently to a conserved cysteine residue in the N-terminus of *Agrobacterium* phytochrome Agp1. *Biochemistry* 43: 3659 – 3669

22. Otero LH, Klinke S, Rinaldi J, Velazquez-Escobar F, Mroginski MA, Fernandez Lopez M, Malamud F, Vojnov AA, Hildebrandt P, Goldbaum FA *et al* (2016) Structure of the full-length bacteriophytochrome from the plant pathogen *Xanthomonas campestris* provides clues to its long-range signaling mechanism. *J Mol Biol* doi: 10.1016/j.jmb.2016.04.012

23. Moglich A, Ayers RA, Moffat K (2009) Structure and signaling mechanism of Per-ARNT-Sim domains. *Structure* 17: 1282 – 1294

24. Rottwinkel G, Oberpichler I, Lamparter T (2010) Bathy phytochromes in rhizobial soil bacteria. *J Bacteriol* 192: 5124 – 5133

25. Karniol B, Vierstra RD (2003) The pair of bacteriophytochromes from *Agrobacterium tumefaciens* are histidine kinases with opposing photobiological properties. *Proc Natl Acad Sci USA* 100: 2807 – 2812

26. Underwood W, Melotto M, He SY (2007) Role of plant stomata in bacterial invasion. *Cell Microbiol* 9: 1621 – 1629

27. Rigano LA, Payette C, Brouillard G, Marano MR, Abramowicz L, Torres PS, Yun M, Castagnaro AP, Oirdi ME, Dufour V *et al* (2007) Bacterial cyclic beta-(1,2)-glucan acts in systemic suppression of plant immune responses. *Plant Cell* 19: 2077 – 2089

28. Yun MH, Torres PS, El Oirdi M, Rigano LA, Gonzalez-Lamothe R, Marano MR, Castagnaro AP, Dankert MA, Bouarab K, Vojnov AA (2006) Xanthan induces plant susceptibility by suppressing callose deposition. *Plant Physiol* 141: 178 – 187

29. Millet YA, Danna CH, Clay NK, Songnuan W, Simon MD, Werck-Reichhart D, Ausubel FM (2010) Innate immune responses activated in *Arabidopsis* roots by microbe-associated molecular patterns. *Plant Cell* 22: 973 – 990

30. Barber CE, Tang JL, Feng JX, Pan MQ, Wilson TJ, Slater H, Dow JM, Williams P, Daniels MJ (1997) A novel regulatory system required for pathogenicity of *Xanthomonas campestris* is mediated by a small diffusible signal molecule. *Mol Microbiol* 24: 555 – 566

31. Buttner D, Bonas U (2010) Regulation and secretion of *Xanthomonas* virulence factors. *FEMS Microbiol Rev* 34: 107 – 133

32. Torres PS, Malamud F, Rigano LA, Russo DM, Marano MR, Castagnaro AP, Zorreguieta A, Bouarab K, Dow JM, Vojnov AA (2007) Controlled synthesis of the DSF cell-cell signal is required for biofilm formation and virulence in *Xanthomonas campestris*. *Environ Microbiol* 9: 2101 – 2109

33. Rigano LA, Siciliano F, Enrique R, Sendin L, Filippone P, Torres PS, Questa J, Dow JM, Castagnaro AP, Vojnov AA *et al* (2007) Biofilm formation, epiphytic fitness, and canker development in *Xanthomonas axonopodis* pv. citri. *Mol Plant Microbe Interact* 20: 1222 – 1230

34. Malamud F, Torres PS, Roeschlin R, Rigano LA, Enrique R, Bonomi HR, Castagnaro AP, Marano MR, Vojnov AA (2011) The *Xanthomonas axonopodis* pv. citri flagellum is required for mature biofilm and canker development. *Microbiology* 157: 819 – 829

35. Baptista JC, Machado MA, Homem RA, Torres PS, Vojnov AA, do Amaral AM (2010) Mutation in the xpsD gene of *Xanthomonas axonopodis* pv. citri affects cellulose degradation and virulence. *Genet Mol Biol* 33: 146 – 153

36. Meyer KM, Leveau JH (2012) Microbiology of the phyllosphere: a playground for testing ecological concepts. *Oecologia* 168: 621 – 629

37. Lindow SE, Brandl MT (2003) Microbiology of the phyllosphere. *Appl Environ Microbiol* 69: 1875 – 1883

38. Gunasekera TS, Sundin GW (2006) Role of nucleotide excision repair and photoreactivation in the solar UVB radiation survival of *Pseudomonas syringae* pv. syringae B728a. *J Appl Microbiol* 100: 1073 – 1083

39. Rio-Alvarez I, Rodriguez-Herva JJ, Martinez PM, Gonzalez-Melendi P, Garcia-Casado G, Rodriguez-Palenzuela P, Lopez-Solanilla E (2013) Light regulates motility, attachment and virulence in the plant pathogen *Pseudomonas syringae* pv tomato DC3000. *Environ Microbiol* 16: 2072 – 2085

40. Ricci A, Dramis L, Shah R, Gartner W, Losi A (2015) Visualizing the relevance of bacterial blue- and red-light receptors during plant-pathogen interaction. *Environ Microbiol Rep* 7: 795 – 802

41. Moriconi V, Sellaro R, Ayub N, Soto G, Rugnone M, Shah R, Pathak GP, Gartner W, Casal JJ (2013) LOV-domain photoreceptor, encoded in a genomic island, attenuates the virulence of *Pseudomonas syringae* in light-exposed *Arabidopsis* leaves. *Plant J* 76: 322 – 331

42. de Wit M, Spoel SH, Sanchez-Perez GF, Gommers CM, Pieterse CM, Voesenek LA, Pierik R (2013) Perception of low red: far-red ratio compromises both salicylic acid- and jasmonic acid-dependent pathogen defences in *Arabidopsis*. *Plant J* 75: 90 – 103

43. Hua J (2013) Modulation of plant immunity by light, circadian rhythm, and temperature. *Curr Opin Plant Biol* 16: 406 – 413

44. Griebel T, Zeier J (2008) Light regulation and daytime dependency of inducible plant defenses in *Arabidopsis*: phytochrome signaling controls systemic acquired resistance rather than local defense. *Plant Physiol* 147: 790 – 801

45. Sorhagen K, Laxa M, Peterhansel C, Reumann S (2013) The emerging role of photorespiration and non-photorespiratory peroxisomal metabolism in pathogen defence. *Plant Biol* 15: 723 – 736

46. He YW, Zhang LH (2008) Quorum sensing and virulence regulation in *Xanthomonas campestris*. *FEMS Microbiol Rev* 32: 842 – 857

47. Ryan RP, An SQ, Allan JH, McCarthy Y, Dow JM (2015) The DSF family of cell-cell signals: an expanding class of bacterial virulence regulators. *PLoS Pathog* 11: e1004986

48. Smith H (2000) Phytochromes and light signal perception by plants—an emerging synthesis. *Nature* 407: 585 – 591

49. Cadmus MC, Rogovin SP, Burton KA, Pittsley JE, Knutson CA, Jeanes A (1976) Colonial variation in *Xanthomonas campestris* NRRL B-1459 and

50. characterization of the polysaccharide from a variant strain. *Can J Microbiol* 22: 942 – 948

50. Sherwood MT (1970) Improved synthetic medium for the growth of *Rhizobium*. *J Appl Bacteriol* 33: 708 – 713

51. Malamud F, Homem RA, Conforte VP, Yaryura PM, Castagnaro AP, Marano MR, do Amaral AM, Vojnov AA (2013) Identification and characterization of biofilm formation-defective mutants of *Xanthomonas citri* subsp. citri. *Microbiology* 159: 1911 – 1919

52. Prentki P, Krisch HM (1984) *In vitro* insertional mutagenesis with a selectable DNA fragment. *Gene* 29: 303 – 313

53. Schafer A, Tauch A, Jager W, Kalinowski J, Thierbach G, Puhler A (1994) Small mobilizable multi-purpose cloning vectors derived from the *Escherichia coli* plasmids pK18 and pK19: selection of defined deletions in the chromosome of *Corynebacterium glutamicum*. *Gene* 145: 69 – 73

54. Kovach ME, Phillips RW, Elzer PH, Roop RM II, Peterson KM (1994) pBBR1MCS: a broad-host-range cloning vector. *Biotechniques* 16: 800 – 802

55. Kumar S, Stecher G, Tamura K (2016) MEGA7: molecular evolutionary genetics analysis version 7.0 for bigger datasets. *Mol Biol Evol* 33: 1870 – 1874

56. Whelan S, Goldman N (2001) A general empirical model of protein evolution derived from multiple protein families using a maximum-likelihood approach. *Mol Biol Evol* 18: 691 – 699

57. Letunic I, Bork P (2016) Interactive tree of life (iTOL) v3: an online tool for the display and annotation of phylogenetic and other trees. *Nucleic Acids Res* 44: W242 – W245

58. Klinke S, Otero LH, Rinaldi J, Sosa S, Guimaraes BG, Shepard WE, Goldbaum FA, Bonomi HR (2014) Crystallization and preliminary X-ray characterization of the full-length bacteriophytochrome from the plant pathogen *Xanthomonas campestris* pv. campestris. *Acta Crystallogr F Struct Biol Commun* 70: 1636 – 1639

59. Vojnov AA, Zorreguieta A, Dow JM, Daniels MJ, Dankert MA (1998) Evidence for a role for the gumB and gumC gene products in the formation of xanthan from its pentasaccharide repeating unit by *Xanthomonas campestris*. *Microbiology* 144: 1487 – 1493

60. Malamud F, Conforte VP, Rigano LA, Castagnaro AP, Marano MR, Morais do Amaral A, Vojnov AA (2012) HrpM is involved in glucan biosynthesis, biofilm formation and pathogenicity in *Xanthomonas citri* ssp. citri. *Mol Plant Pathol* 13: 1010 – 1018

61. Heydorn A, Nielsen AT, Hentzer M, Sternberg C, Givskov M, Ersboll BK, Molin S (2000) Quantification of biofilm structures by the novel computer program COMSTAT. *Microbiology* 146 (Pt 10): 2395 – 2407

62. Ortiz G, Blasco M, Albertó E (2016) An economical and high throughput alternative for endoglucanase activity determination. *BioTechnology — An Indian Journal* 12: 70 – 74

63. Bolger AM, Lohse M, Usadel B (2014) Trimmomatic: a flexible trimmer for Illumina sequence data. *Bioinformatics* 30: 2114 – 2120

64. Li H, Handsaker B, Wysoker A, Fennell T, Ruan J, Homer N, Marth G, Abecasis G, Durbin R (2009) The sequence alignment/map format and SAMtools. *Bioinformatics* 25: 2078 – 2079

65. Li H, Durbin R (2009) Fast and accurate short read alignment with Burrows-Wheeler transform. *Bioinformatics* 25: 1754 – 1760

66. Liao Y, Smyth GK, Shi W (2014) FeatureCounts: an efficient general purpose program for assigning sequence reads to genomic features. *Bioinformatics* 30: 923 – 930

67. Anders S, Huber W (2010) Differential expression analysis for sequence count data. *Genome Biol* 11: R106 .